COMMUNICATION

Lithium extraction using zirconium oxide coated lithium manganese oxide ion-exchange adsorbents†

Karthik Ramachandran Shivakumar, [iD][a] Ashkan Zolfaghari,[ab] Salman Safari, [iD][ac] Fangshuai Wu, [iD][a] Brendan A. Bishop, [iD][d] Ning Chen, [iD][e] Leslie J. Robbins [iD][d] and Daniel S. Alessi [iD]*[a]

Lithium extraction from sedimentary brines using spinel lithium manganese oxide, $Li_{1.6}Mn_{1.6}O_4$, is challenging because of the presence of dissolved organic compounds, resulting in manganese reduction and loss. Coating the sorbent with a 7.5 nm layer of zirconium dioxide decreased manganese loss by approximately 50%, while not substantially impacting its adsorption capacity and selectivity, thereby increasing its usable life.

Driven by policies aimed at transitioning away from internal combustion engines, the demand for lithium (Li), a crucial component of electric vehicle (EV) batteries, is projected to increase in the coming decades.[1,2] To satisfy this rapidly increasing demand,[3] Vera *et al.* recommended the development of technologies to extract Li from alternative sources.[4] Elevated Li concentrations have been discovered in formation waters from sedimentary basins where concentrations can exceed 75 ppm, hereafter termed formation water type lithium bearing waters (f-LBW).[5] While many of these basins contain elevated Li concentrations,[1,6] wells with over 75 mg L^{-1} generally occur in fluids with over 100 000 mg L^{-1} total dissolved solids (TDS) at depths greater than one kilometer.[5] The conventional Li evaporation process applied to continental, or salar, brines is slow and time consuming, with production times between 10–24 months.[4] This technology cannot be applied to extract Li from f-LBW because of the low Li concentrations, high Mg/Li ratios, and unsuitable climactic conditions in many regions.[7] Ion-exchange adsorbents are effective in extracting Li from f-LBW, with production times between a few hours to days. Among these, spinel lithium manganese oxide (LMO; $Li_{1.6}Mn_{1.6}O_4$) adsorbents have the highest Li extraction capacity, rapid lithiation kinetics, and high Li selectivity.[8,9] For example, LMO was able to extract 80% of the Li in a sedimentary brine containing 43 mg L^{-1} Li over 30 min at a wellhead water temperature of 70 °C, with a resulting Li uptake capacity of 18 mg g^{-1}.[9]

One of the disadvantages of using LMO type adsorbents, however, is adsorbent loss during Li extraction from the brine. This is due to the formation of Mn^{3+} ions during Li intercalation into LMO, a result of the Jahn–Teller effect, and the subsequent disproportionation of Mn^{3+} during protonation that results in the production and dissolution of Mn^{2+} (Mn-loss).[10,11] In addition to inherent Mn-loss due to the Jahn–Teller effect, sedimentary LBWs often contain complex dissolved organic compounds (DOC), including polycyclic aromatic hydrocarbons (PAH), polyethylene glycols (PEG), octylphenol ethoxylates (OPE), and other reducing agents like H_2S, leading to further Mn-loss.[12] These organic compounds may react with the surface of LMO nanoparticles and aggregates during Li extraction, reducing Mn^{4+} on the surface, and resulting in increased Mn^{3+} formation and eventual disproportionation and dissolution as Mn^{2+}. This type of Mn-loss is usually 5 to 10 times higher in f-LBW than the Mn-loss observed in simulated LiCl solutions.[9,13] Seip *et al.*[9] showed that reduced Mn^{3+} during Li extraction changed the average Mn–Mn distance in the LMO lattice. Such structural changes currently limit the application of LMO in commercial operations, as they have poor recyclability when used in f-LBW.

Herein, we address the Mn-loss problem in f-LBW by coating the LMO surface with ZrO_2 using a solvent evaporation–crystallization method. This thin coating on the adsorbent acts as a physical barrier, separating LMO from DOC in solution (Fig. S1, ESI†). Various ZrO_2 coating thicknesses were tested, and Li adsorption data were analysed to determine the impact of coating thickness on Li uptake capacity and Mn-loss. Results

[a] *Department of Earth and Atmospheric Sciences, University of Alberta, 1-26 Earth Sciences Building, Edmonton, Alberta T6G 2E3, Canada.*
  E-mail: alessi@ualberta.ca
[b] *Suncor Energy Inc, Calgary, Alberta, Canada*
[c] *CANDLE Lithium Corporation, Edmonton, Alberta T5S 1G4, Canada*
[d] *Department of Earth Sciences, University of Regina, 3737 Wascana Parkway, Regina, SK S4S 0A2, Canada*
[e] *Canadian Light Source Inc., University of Saskatchewan, 114 Science Place, Saskatoon S7N 2V3, Saskatchewan, Canada*
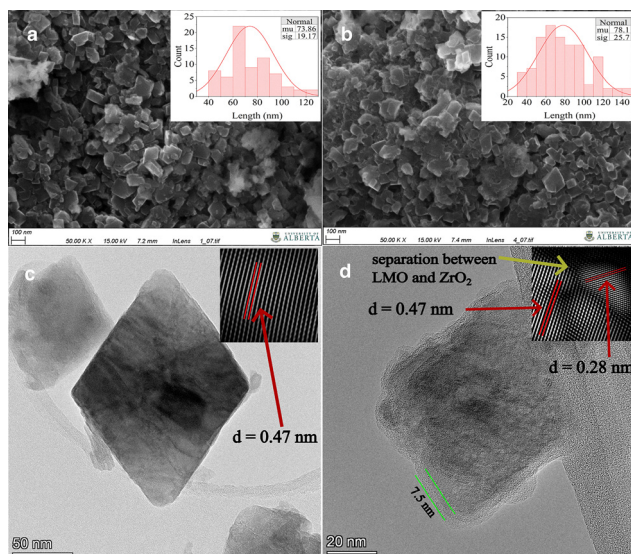
Fig. 1 Scanning electron microscopy (SEM) images of (a) bare LMO and (b) 7.5 nm LMO with inset images indicating the particle size distribution. HR-TEM images of (c) bare LMO and (d) 7.5 nm LMO.

Fig. 2 (a) Correlation between coating thickness to Li uptake and Mn-loss after the first cycle in f-LBW. The relationship between adsorbent particle size on Li uptake and Mn-loss for (b) bare LMO, (c) 1.5 nm LMO, and (d) 7.5 nm LMO, with their respective fits indicating linear correlations.

showed that the coated adsorbent had markedly decreased Mn-loss, with negligible decreases in Li uptake and increased recyclability. With brines that have low concentrations of DOC and high Li concentrations, the ZrO_2 coated LMO adsorbent has higher Li uptake capacity, significantly lower Mn-loss, and higher recyclability, factors critical for improving the economics of Li recovery in processes using ion-exchange type DLE for f-LBW.

The synthesized bulk pristine bare LMO contained aggregates of different sizes ranging from 75 μm to 2 mm. The SEM image of LMO showed heterogeneous nanoparticles ranging from 40 nm to 90 nm. Comparison of the 75 μm LMO particles showed that the surface of the bare LMO and the 7.5 nm coated LMO had similar particle sizes, with ZrO_2 coated LMO particles appearing to have fused together as the coating acted as a binder (Fig. 1). The *d*-spacing of the lattice fringes of the bare LMO was 0.47 nm, which did not change after coating (Fig. 1). The ZrO_2 region, having a distinctive *d*-spacing of 0.28 nm, showed a coating layer on top of the cubic LMO particles.[14] The HR-TEM image of pristine coated LMO (Fig. S3, ESI†) showed that a ZrO_2 coating layer had formed on top the LMO crystal with thicknesses ranging from 6 nm to 10 nm, and averaging approximately 7.5 nm. Particle size distribution analysis (Fig. 1a and b inset graphs) showed that the average particle size had increased slightly from 73 nm to 78 nm after coating. The BET surface area of bare LMO was 144 m^2 g^{-1} and of the 7.5 nm coated LMO was 40 m^2 g^{-1}. The reduction in BET surface area can be directly attributed to the ZrO_2 coating, which bound LMO particles together.

Lithium adsorption tests using <75 μm LMO particles in simulated LBW (100 mg per L Li) demonstrated that increases in the coating thickness from 0 to 7.5 nm did not have a significant impact on the Li uptake capacity, while Mn-loss decreased slightly from 0.8% to 0.6% (Fig. S4, ESI†). These
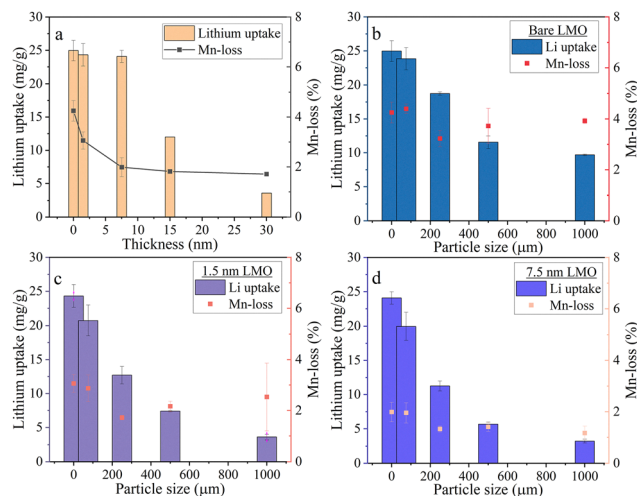
Mn-loss results were consistent with Wang et al.,[15] where the coating layer acts as barrier to redox reactions and the Li uptake capacity did not change substantially as the porous structure of the ZrO_2 coating permits Li ion diffusion. In f-LBW (Fig. 2a), increasing the coating thickness from 0 to 7.5 nm did not impact the Li uptake capacity, and Mn-loss decreased from 4.2% to 2%. Mn-loss in f-LBW was 80% higher than in simulated LBW because of the presence of Mn-reducing organic compounds in f-LBW. The Mn-loss for coated LMO decreased compared to bare LMO because the physical barrier provided by the ZrO_2 coating separates the LMO surface and the DOC in f-LBW. Xue et al.[14] showed that thicker coatings decrease Li uptake capacity. Consistent with this observation, increasing the coating thickness further to 30 nm caused the Li uptake capacity to decrease from 25 mg g^{-1} to 2.5 mg g^{-1} likely because the ZrO_2 coating blocked Li$^+$ diffusion pathways, while Mn-loss did not decrease further. Thus, the optimal coating range was determined to be between 1.5 nm and 7.5 nm, where we observed minimal loss in Li uptake and a significant decrease in Mn-loss.

Lithium extraction studies using bare LMO in f-LBW showed that the Li uptake capacity was negatively correlated with the LMO particle size (Fig. 2b). Thus, the particles were categorized by size before coating them with ZrO_2. Based on the relationship between ZrO_2 coating thickness and Li uptake/Mn-loss (Fig. 2a), two different coating thicknesses (1.5 nm and 7.5 nm) were studied to find the particle size having an optimal Li uptake capacity and Mn-loss. For bare LMO, increasing the particle size resulted in an exponential decrease in Li uptake capacity (Fig. 2b). The larger particles were aggregates with less contact surface area with f-LBW, resulting in slower Li$^+$ diffusion. The Mn-loss for the bare LMO remained nearly the same for all particle sizes observed after the first cycle. For the 1.5 nm coated and 7.5 nm coated LMO, the Li uptake capacity was reduced by only 4% for <75 μm particles, whereas there was

greater than 70% reduction in Li uptake capacity for the 1000 μm particles coated with 1.5 nm and 7.5 nm ZrO_2 (Fig. 2c and d) likely due to diffusion limitations caused by the coating.

The ZrO_2 coating negatively impacted larger adsorbent particles to a greater extent than for smaller particle sizes. Mn-loss was reduced by 30% and 53% with 1.5 nm and 7.5 nm ZrO_2 coatings, respectively, for the <75 μm particle size and this did not improve further with larger particle sizes after the first cycle, because the ZrO_2 acted as a physical barrier to the reducing agents in f-LBW. Smaller LMO particles have slightly higher Mn-loss likely due to the larger specific surface area that facilitated reductive dissolution of the adsorbent.[9] In summary, <75 μm particles having a 7.5 nm ZrO_2 coating yielded an optimal balance between maintaining Li uptake and preventing Mn loss.

Approximately 4% Mn-loss per cycle was observed when the bare LMO was repeatedly exposed to f-LBW (Fig. 3a). After 4 cycles, this loss amounted to nearly 16% of the initial Mn. This loss decreased by 30% and 50% for the 1.5 nm and 7.5 nm coated LMO, respectively, indicating that the 7.5 nm coated LMO sample had higher recyclability than bare LMO.[15] No change in the average Li uptake capacity between cycles was observed for the 1.5 nm LMO. Mn-loss was less than 3% for the first three cycles but after the fourth cycle the Mn-loss was nearly 4%, indicating degradation of the coating layer, consistent with the 0.02% Zr^{4+} loss per cycle. The LMO with a 7.5 nm coating had a maximum Li extraction capacity of 24 mg g^{-1} after 1 h of extraction at room temperature. A slight 4% reduction in Li uptake capacity was noted after 4 cycles of operation. On average, for the 7.5 nm coating, LMO Mn-loss was less than 2% during all four cycles, while the Zr-loss of pristine 7.5 nm LMO was less than 0.6% after being exposed to 0.5 M HCl for 10 h (Fig. S5, ESI†), and 10.2% when exposed to a 6 M HCl + 30% H_2O_2 solution. This indicated that the 7.5 nm LMO was more resistant to mechanical and chemical degradation than the bare LMO. The Li regeneration after every cycle was greater than 80%.
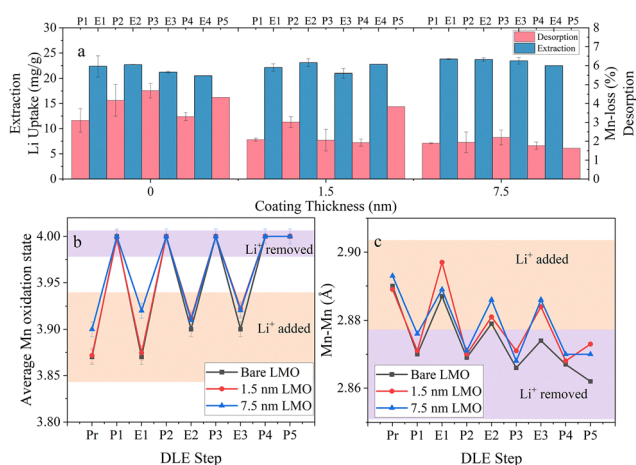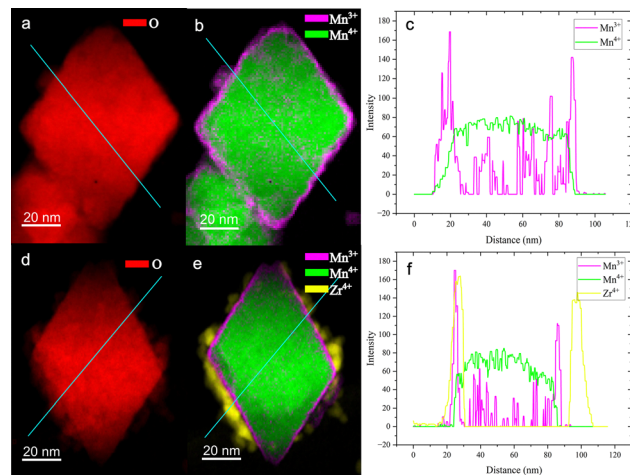

Fig. 4 O, Mn(III), Mn(IV), and Zr(IV) TEM-EELS mapping and line spectra of (a)–(c) bare LMO after one cycle and (d)–(f) 7.5 nm coated LMO after one cycle.

TEM-EELS visualization of the spatial distribution of Mn in LMO during Li extraction from f-LBW showed that a layer of Mn^{3+} had formed on the surface of the samples (Fig. 4). Consistent with Seip et al.,[9] the formation of this layer indicated that Mn^{4+} on the surface was reduced to Mn^{3+} as a direct result of contact with reducing agents in f-LBW. Mn^{3+} production in bare LMO (Fig. 4b) primarily occurred on the surface but was also present throughout the sample. The ratios of Mn^{4+} and Mn^{3+} species on the line spectra (Fig. 4c) also confirmed this hypothesis. In 7.5 nm coated LMO, the reduction of Mn^{4+} at the surface and within the bulk phase decreased significantly. The presence of a 7.5 nm ZrO_2 coating on top of the LMO was also confirmed using TEM-EELS (Fig. 4e). After 4 extraction cycles (Fig. S7, ESI†), the distribution of Mn^{3+} in the 7.5 nm ZrO_2 coated LMO resembled that of the bare LMO, likely because of significant damage of the oxygen in the LMO framework.

Comparison of the XANES spectra of the lithiated and protonated samples show three distinct spectral features (Fig. S8, ESI†). The pre-edge peaks between 6535 and 6545 eV are similar to peaks on the spinel compounds and represent dipole-forbidden transitions responsible for 1s to $3d_{t_{2g}}$ (A1) and 1s to $3d_{e_g}$ (A2) states.[16] The absorption edge arises from the 1s to 4p orbital transition and the features on the edge are the result of medium to long range order in the spinel (B1, B2) and contraction and expansion of the unit cell (C1, C2). Comparing the sample spectra during the extraction and protonation cycles to those of reference materials, the absorption edge shifted to the left and right, respectively. Specifically, based on the XANES spectra of the bare LMO, there was a shift in position of the C1 and C2 features to a higher energy in extracted samples and to a lower energy in protonated samples. This is indicative of resonating expansion and contraction of the unit cell during extraction (lithiation) and protonation (delithiation).[17] However, as the bare LMO aged, a shift to higher energy in the extracted samples was also observed. This change is not reversible, unlike the resonating unit cell observed between the

Fig. 3 (a) Cycle testing, (b) oxidation state, and (c) change in Mn–Mn distance of bare LMO, 1.5 nm LMO, and 7.5 nm LMO after cycles 1, 2, 3, and 4.

extracted and protonated states. There was minimal change in the C1 and C2 feature for the 1.5 and 7.5 nm ZrO_2 coated LMO, confirming retention of the unit cell volume. This type of shift provided evidence of structural damage in the spinel structure of the bare LMO after four cycles. The expansion of the unit cell with further DLE cycles did not impact the protonation state, likely one of the reasons that the bare LMO retained its Li uptake capacity.

Linear combination fitting (LCF) of the reference materials spectra to the bare LMO, 1.5 nm LMO, and 7.5 nm LMO spectra (Table S3, ESI†) showed that the spectra of all LMO types were similar to the XANES spectra of the spinel reference materials ($LiMn_2O_4$ and $Li_{1.33}Mn_{1.67}O_4$). Combined with TEM-EELS Mn mapping, we infer that most of the Mn in the spinel was in the Mn^{4+} state. Thus, by using protonated spinel reference materials and a Mn^{3+} reference material (Mn_3O_4), the average oxidation state of the LMO samples could be monitored across DLE cycles. The bare LMO showed at least 10% transformation of spinel Mn^{4+} to Mn^{3+} each cycle.

The oxidation state (Fig. 3b) of the pristine bare LMO was determined as +3.87 and for 7.5 nm LMO, +3.90.[18] This slight increase in oxidation state could be the result of the second calcination step after ZrO_2 coating, where more oxygen was available for oxidation of Mn^{3+} in the LMO present initially as an impurity. The oxidation state of all the protonated samples was +4, indicating complete disproportionation of Mn^{3+} by the protonation acid.[17–19] After coating with 7.5 nm ZrO_2, the oxidation states of the extracted samples increased, indicating decreased Mn^{3+} formation every cycle.

Comparison of the EXAFS spectra between the first and the third extraction cycles (Fig. S10a, ESI†) and first protonation and fifth protonation cycles (Fig. S10c, ESI†) reveals a slight change in the second maxima (2.3 Å) in the R-space for bare LMO, but for 7.5 nm LMO showed no noticeable shift (Fig. S10b, and d ESI†). The absence of the shoulder peak and the subsequent change in position and shape of the following peaks indicated structural changes in the spinel which are probably caused by the reductive dissolution of Mn^{3+}. The change in the spectra beyond 3 Å in the cycled protonated sample also indicated structural changes in the MnO_6 octahedron. Both extracted and protonated versions of the 7.5 nm LMO (Fig. S10b and d ESI†) did not show changes in the R-space peaks.

The EXAFS fit results (Table S4, ESI†) indicated minimal change in the first shell (Mn–O) distances for all samples. The average Mn–Mn second shell distance changed during Li extraction and protonation (Fig. 3c). The reversible alteration in the Mn–Mn distance was likely due to the formation of Mn^{3+} ions during Li^+ extraction. The Mn^{4+}–Mn^{3+} bond is longer than the Mn^{4+}–Mn^{4+} bond, which caused the observed increase in average Mn–Mn distance during Li^+ extraction.[17] The bare LMO began to deteriorate after 3 cycles of DLE operation, consistent with the Mn–Mn distance of less than 2.87 Å after protonation and the fact that the spinel did not recover to the original state

(Mn–Mn distance of 2.87 Å). The decrease in the Mn–Mn distance is attributed to the decrease in the total Mn species present in LMO, caused by reductive dissolution. Shortening of Mn–O and Mn–Mn distances may result in a phase change from cubic spinel to tetragonal spinel, reducing the recyclability of the bare LMO.[20] In the coated LMO sample, the Mn–Mn distance partially recovered in 1.5 nm LMO and fully recovered in 7.5 nm LMO (Fig. 3c), indicating that life cycle of the LMO can be increased using ZrO_2 coatings and are effective in Li extraction from f-LBW.

We coated LMO with different thicknesses of ZrO_2 using an evaporative crystallization method. The coating layer did not impact the Li^+ adsorption from LBW, but significantly lowered Mn-loss when compared to the bare LMO. By optimizing the coating thickness for Li uptake and Mn-loss, the 7.5 nm coated LMO had the highest Li uptake capacity, 24 mg g^{-1}, and a lower Mn-loss of 2% per cycle. This increased performance improves the recyclability and economics of an LMO-based DLE process, particularly when this adsorbent is used in f-LBW containing Mn-reducing agents. Our results contribute to effectively establishing the mineral and economic potential of low-lithium bearing sedimentary brines, supporting the clean energy transition and expressed climate change goals.

Conflicts of interest

There are no conflicts to declare.

Data availability

The data supporting this article have been included as part of the ESI.†

Notes and references

1 C. Xu, *et al.*, *Commun. Mater.*, 2020, **1**, 1–10.
2 B. Jones, *et al.*, *Appl. Energy*, 2020, **280**, 115072.
3 F. Maisel, *et al.*, *Resour., Conserv. Recycl.*, 2023, **192**, 106920.
4 M. L. Vera, *et al.*, *Nat. Rev. Earth Environ.*, 2023, **4**, 149–165.
5 A. Ettehadi, *et al.*, *Energy Fuels*, 2024, **38**(12), 10517–10541.
6 M. Marza, *et al.*, *J. Geochem. Explor.*, 2024, **257**, 107383.
7 Y. Ogawa, *et al.*, *Res. Geol.*, 2014, **64**, 91–101.
8 R. Chitrakar, *et al.*, *Ind. Eng. Chem. Res.*, 2001, **40**, 2054–2058.
9 A. Seip, *et al.*, *Chem. Eng. J.*, 2021, **426**, 130713.
10 J. B. Goodenough, *Annu. Rev. Mater. Sci.*, 1998, **28**, 1–27.
11 G. Zhang, *et al.*, *Chem. Eng. J.*, 2022, **450**, 137912.
12 E. J. Folkerts, *et al.*, *Ecotoxicol. Environ. Saf.*, 2019, **180**, 600–609.
13 G. Zhang, *et al.*, *Colloids Surf.*, 2021, **629**, 127465.
14 F. Xue, *et al.*, *Desalination*, 2024, **574**, 117290.
15 L. Wang, *et al.*, *Sep. Purif. Technol.*, 2022, **303**, 121933.
16 T. Kim, *et al.*, *Chem. Mater.*, 2016, **28**, 4191–4203.
17 M. J. Ariza, *et al.*, *Chem. Mater.*, 2006, **18**, 1885–1890.
18 R. Chitrakar, *et al.*, *Chem. Mater.*, 2000, **12**, 3151–3157.
19 R. Chitrakar, *et al.*, *J. Solid State Chem.*, 2002, **169**, 66–74.
20 J. B. Falqueto, *et al.*, *J. Mater. Chem. A*, 2023, **11**, 24800–24811.